Soft Computing (2022) 26:3385–3399
https://doi.org/10.1007/s00500-022-06749-x

OPTIMIZATION

Modelling and optimization of weld bead geometry in robotic gas metal arc-based additive manufacturing using machine learning, finite-element modelling and graph theory and matrix approach

K. Venkata Rao[1] · Satish Parimi[1] · L. Suvarna Raju[1] · Gamini Suresh[1]

Accepted: 2 January 2022 / Published online: 15 January 2022

Abstract
The objective of this study is to investigate effects of the welding speed, wire feed speed, and torch angle on the weld geometry, including height, width, and depth of metal deposition, in additive manufacturing of mild steel. In the present study, artificial neural network was developed to predict weld bead geometry and validate the optimization of process parameters to improve quality of weld bead geometry. Experimental results for the width, depth, and height of the weld bead geometry were collected, and the interaction effect of the process parameters on the weld bead geometry was investigated. Three-dimensional finite-element modelling was performed for the AM, and the width, depth, and height of the weld geometry were predicted. The Taguchi method-based graph theory and matrix approach and the utility concept were used to optimise the process parameters for achieving the dimensional accuracy in AM. The optimal working condition was as follows: a torch angle of 60°, a wire feed speed of 6 m/min, and a welding speed of 0.4 m/min. Under the optimal working conditions, the height, width, and depth of the weld bead were 3.910, 7.615, and 2.000 mm, respectively. The optimization was also validated with ANN and a comparison among the ANN, simulation and experimental results revealed good agreement.

Keywords Additive manufacturing · ANN · Numerical simulation · Weld geometry · Robot-based GMAW

1 Introduction

Robotic gas metal arc welding (GMAW)-based additive manufacturing (AM) is an emerging technology for the fabrication of large and complex components. AM is widely used to fabricate three-dimensional objects layer-by-layer. The AM technique is completely different from conventional manufacturing and reduces the amount of material wasted, with a production efficiency of approximately 75%–85%. There are three types of wire arc AM methods with different heat sources: GMAW, gas tungsten arc welding, and plasma arc welding. Among them, GMAW is often used when the objects are fabricated with metal (Majeed et al. 2020). In most cases, GMA-based AM is performed using articulated industrial robots, and the arc path is guided by the robot. GMAW is in the category of cold metal transfer, which reduces the processing heat input at high frequencies (Azar 2015). This technique is associated with high deposition rates, low cost, and good structural integrity throughout the object. Various products, including Ti-6Al-4 V spare parts, steel wind tunnels, and aluminium wing ribs, are manufactured via this process (Williams et al. 2016). The dimensional accuracy of the wall geometry in terms of width, depth and height and surface quality is still big challenge to manufactures to obtain the parts with a tight tolerance range. To overcome these difficulties, the weld bead is controlled by adjusting the process parameters.

Manufacturing of parts is associated with shorter product life cycle, on demand production and sustainability. Among the conventional manufacturing methods, the AM is an example of that kind. The AM technique is used to directly fabricate thin-walled components. As AM is an emerging technique, there are many issues and difficulties

✉ K. Venkata Rao
kvenkatrama@gmail.com; kvenkat_rama@rediffmail.com

[1] Department of Mechanical Engineering, Vignan's Foundation for Science, Technology and Research, Vadlamudi, India

associated with this method. In AM, it was observed that the weld bead geometry is not uniform at the starting and ending of the weld bead. Hu et al. (2018) reported that there is a backward flow of the metal in the weld pool as the arc flow in the forward direction results in an abnormal weld bead at the starting and ending, such as swelling at the starting and reduction at the ending. They adjusted the process parameters to control the weld bead throughout the length and optimised the process parameters to obtain a uniform bead at the starting ending of the bead. At high wire feed rates, the molten pool became unstable because of the impact of the arc force; additionally, this led to low-quality fabrication. Li et al. (2019) studied the effect of the gas metal arc torch angle on the weld pool stability and developed a method for changing the torch angle. They performed experiments at different torch angles ranging from 45° to 135°. The pool stability was improved by keeping the torch angle smaller than 90°.

As the AM system fabricates the products in layers, the wall layer thickness and depth must be controlled to achieve the required quality. Zhao et al. (2018) studied effect of process parameters such as welding voltage, wire feed speed, welding speed and standoff distance on weld bead geometry in AM. They also optimized process parameters using an adaptive grey wolf algorithm and obtained required height, width and depth of weld bead. Liu et al. (2019) developed a closed-loop quality control system along with an online image acquisition system to control process parameters. The proposed control system analyzed images and adjusted the process parameters and improved the quality of wall geometry. Jin et al. (2017) optimized process planning to reduce metal consumption during the AM. They developed a skeleton-based path planning technique with narrow bead geometry and improved metal deposition efficiency. Gokhale et al. (2019) studied effect of torch angle, welding speed, wire feed speed and current on wall width and height in AM and optimized the process parameters to reduce wall thickness and increase height of the wall. They concluded that width of the wall increased as angle of the torch was increased and at the same time, height of the wall was found to be reduced. Zhao et al. (2011) studied the effect of the heat source on the fabrication of a thin-walled component using finite-element modelling (FEM). It was concluded that the remelting of the single bead in each layer results in a large molten pool and deep penetration.

GMAW is a complex process in AM that involves the interaction of the arc plasma and the arc heat input, the formation of a drop from the molten metal of the electrode, and penetration on the substrate of the plate. As shown in Fig. 1, the filler material is melted, and a weld pool is formed on the plate substrate owing to the interaction of the plasma arc and the arc heat input. The molten metal is

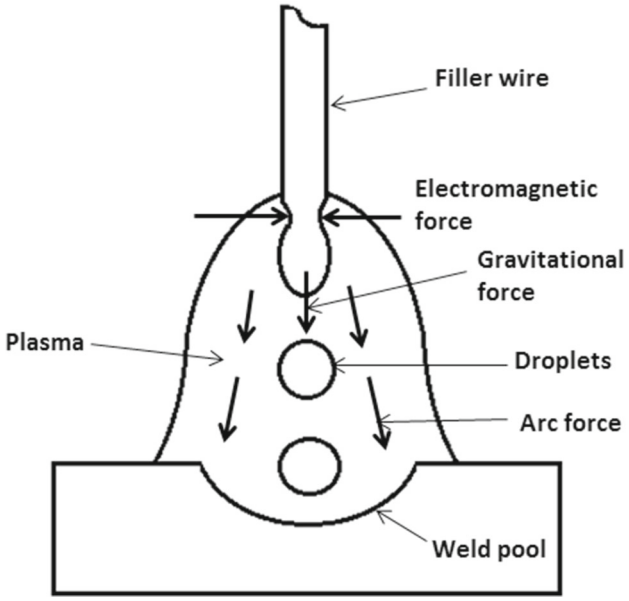

Fig. 1 Schematic of the weld pool and driving forces

separated from the filler wire in the form of a droplet by an electrostatic force and penetrates the substrate on the plate (Wu et al. 2017). Modelling the AM process is an effective way to simulate the wire arc AM for elucidating the process and optimising the sequences of layer deposition during the process. The numerical simulation facilitates the optimisation of important process parameters, such as the heat source power, path of metal deposition, and deposition intervals (Oyama et al. 2019). Researchers have used different modelling techniques to simulate the AM process for different metals. Oyama et al. (2019) performed numerical simulations for AM of Al-5 Mg and Al-3Si alloys to optimise the heat source used for the metal deposition and validated the results experimentally. They proposed an analytical method to estimate the heat input reduction coefficient for experiments as well as simulations. Graf et al. (2018) used FEM-based simulation to predict the temperature, mechanical properties, wall geometry, and distortion in AM. It was concluded that an uniform wall geometry was obtained with a continuous welding path.

It is very difficult to understand and analyse the stability of the weld pool, heat input, and fluid flow during the welding process. Goldak et al. (1984) developed computational fluid dynamics models to investigate the weld pool and fluid flow. Goldak's double-ellipsoidal volume heat source is proposed in modelling of GMAW. Hu et al. (2018) used the Simufact Welding software for GMAW to understand and overcome difficulties in AM.

Qi et al. (2019) stated that the FEM-based models are physics-driven models and are not able to predict the wall geometry quickly. Data-driven models like machine learning (ML) techniques are widely used to overcome the

difficulties associated with the above-said models. The ML techniques like artificial neural network (ANN) and deep learning do not require any physics-based equations; instead, a relationship between the input variables and output targets is developed using the past experimental data to predict the output targets quickly (2016). Baturynska and Martinsen (Kucukoglu et al. 2018) made a comparison between ML algorithms and linear regression models with respect to prediction of wall geometry. They concluded that the ML algorithms have outperformed in prediction of height and length of wall. The ANN is one of the ML techniques widely used in AM due to its strong computational power. Chowdhury et al. (2018) developed an ANN-based geometric compensation methodology to predict optimal part-built orientation in AM. They proposed two stages: in the first stage, a weighted optimization technique was used to optimize process parameters and then validated with the ANN model in the second stage. Garland et al. (2020) used the ML technique to predict dimensional accuracy of 3D printed lattices and concluded that the ML techniques are fast and inexpensive in prediction of wall geometry in AM. It is summarized that the ML techniques are able to predict the output targets easily with shorter time.

In AM, it is necessary to fabricate thin-walled components with the maximum height and minimum width and depth of metal deposition. In addition, it is also required to achieve less cost and shorter time of the process. To achieve the required output characteristics, the process parameters are optimised using different techniques, such as the Taguchi method, response surface methodology, grey relational analysis, and particle swarm optimisation. Cheema et al. (2013) and Venkatarao (2019) reported that the handling of the conventional optimisation techniques becomes complex and confusing in multiresponse optimization. As these optimisation techniques give equal weights to all the output characteristics during multiresponse optimisation, it is impossible to optimise the process parameters when the output characteristics have different preferences (weights). To overcome these difficulties, a new approach that combines the Taguchi method-based graph theory and matrix approach (GTMA) and the utility concept is used in different applications to optimise the process parameters.

As AM is an emerging technology, there are many difficulties related to process and quality control, and it is difficult to understand the process. In the present study, the torch angle was set as 60°, 90°, and 120° to examine the weld bead geometry. The effects of the welding travel speed, wire feed speed, and torch angle on the weld bead geometry (e.g. the width, height, and depth of the weld bead) were examined. Experiments were conducted with different process parameters, and the width, height, and depth of the weld bead were measured. An ANN-based prediction model was developed to predict the width, height, and depth of the weld bead. In addition to that, an FEM-based numerical simulation was also performed to predict the width, height, and depth of the weld bead. The ANN and simulation results were compared with the experimental results, and the effect of the weld pool on the weld geometry was examined. Additionally, the Taguchi method-based GTMA and the utility concept were used to optimise the process parameters for achieving the maximum process performance and the optimization was confirmed by the ANN Technique.

2 FEM of AM

In the present study, the robot-assisted GMA-based AM was modelled, and the results were simulated using the SIMUFACT.WELDING software. This is one of the commercial FEM software packages used to simulate welding characteristics (Knowledge based design advisory system for multi-material joining 2019). Figure 2 shows the FEM of AM on a mild steel substrate with a mild steel filler metal. During the FEM, one metal plate, one bearing, four clamps, and one robot were selected as components for the simulation. In the next step, mild steel is assigned to the plate and filler metal. The steel plate with a size of $150 \times 150 \times 5$ mm^3 was taken as the substrate on the bearing. The substrate was rigidly held on the bearing using clamps, which were positioned at the four corners with a distance of 20 mm from the edges. The metal deposition trajectory and its length were defined on the substrate, as shown in Fig. 2. The AM configuration was modelled with 45,282 elements, and the length, width and height of each element were 0.6, 0.9 and 0.7 mm, respectively. Properties of mild steel were selected from the software library. The melting temperature and the room temperature were assumed to be 1500 °C and 20 °C, respectively. The latent heat during the solidification, Stefan–Boltzmann constant emission coefficient and heat transfer coefficient were 256.4 J/g, 0.6, and 20 W/(m^2 K), respectively. The welding parameters, such as the current, voltage, welding efficiency, welding traverse speed, wire feed speed, and gas flow rate, were defined. In the present study, the current, voltage, gas flow rate, and welding efficiency were 150 A, 20 V, 25 L/min, and 0.85, respectively, for the twenty-seven experiments. The welding speed, wire feed speed, and torch angles and their levels are presented in Table 2.

2.1 Heat-source modelling

During the simulation, the heat source is defined using Goldak's double-ellipsoid model to simulate the weld bead,

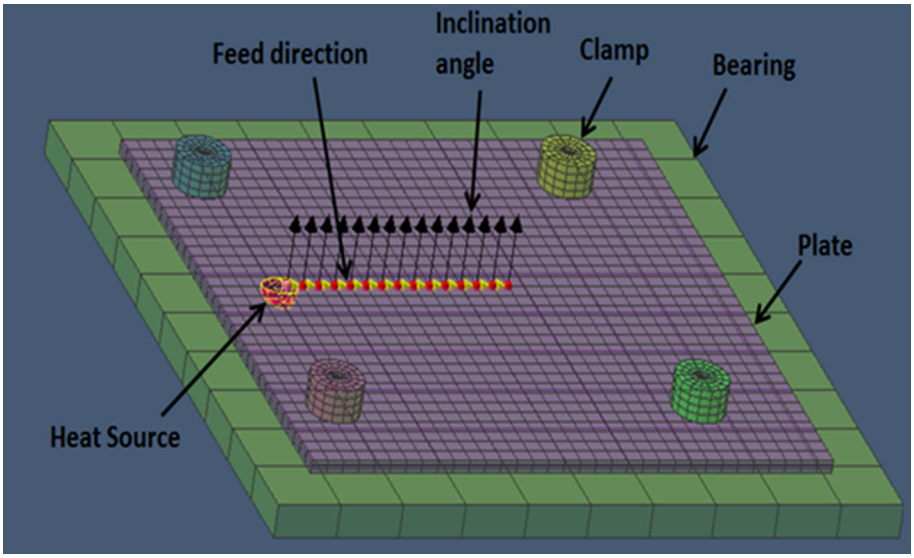

Fig. 2 FEM of AM

as shown in Fig. 3 (Goldak et al. 1984). In the model, the front length, rear length, width, and depth are defined as (a_f), (a_r), (b) and (d), respectively, for the simulation of the metal deposition on the substrate. The heat distribution during the simulation is described as follows:

$$q_f(x,y,z) = \frac{6\sqrt{3}f_f Q}{a_f bc\pi\sqrt{\pi}} \exp\left(-\frac{3x^2}{a_f^2} - \frac{3y^2}{b^2} - \frac{3z^2}{c^2}\right), \quad x \geq 0 \tag{1}$$

$$q_r(x,y,z) = \frac{6\sqrt{3}f_f Q}{a_f bc\pi\sqrt{\pi}} \exp\left(-\frac{3x^2}{a_r^2} - \frac{3y^2}{b^2} - \frac{3z^2}{c^2}\right), \quad x < 0 \tag{2}$$

$$f_f + f_r = 2, Q = \eta VI, \tag{3}$$

where q_f and q_r represent the heat fluxes at the front and rear semi-ellipsoids, respectively, η represents the efficiency, V represents the voltage, Q represents the heat deposited, f_f represents the fraction of heat deposited in the front region, and f_r represents the fraction of heat deposited in the rear region, which were recommended by Goldak as 0.6 and 1.6, respectively. Based on the arc length, torch angle, heat transfer characteristics of the arc, size of weld pool and the shielding gas (a gas mixture of 95% argon and 5% CO_2), the heat source parameters are summarised (Azar 2015; Goldak et al. 1984) as presented in Table 1.

After the double-ellipsoidal heat-source parameters were defined, the simulation was performed. Figure 4 shows the simulation of the AM on the substrate. After the simulation, the width, height, and depth of the metal deposition were measured, as shown in Table 2.

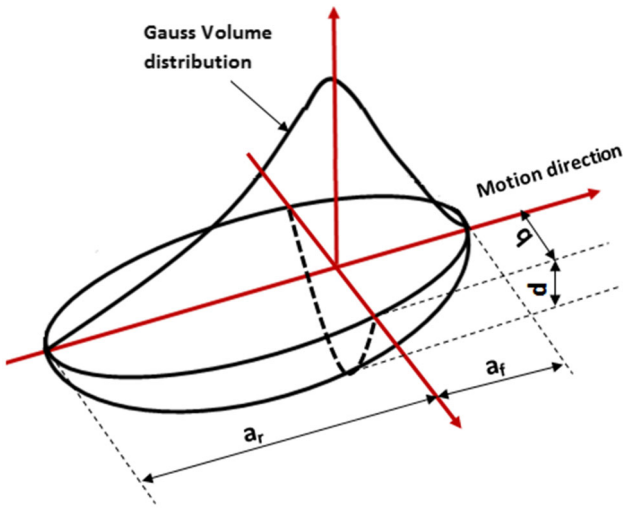

Fig. 3 Double-ellipsoidal heat-source pararmeters

3 Experiments

Figure 5 shows the experimental setup for the robotic AM system using GMAW. In the present study, mild steel as used as the substrate as well as the wire for AM, and 27 experiments were conducted at three levels torch angles (TA), wire feed speeds (WFS), and welding speeds (WS). The mild steel substrate was fixed on a table at a suitable position, and the welding torch was fixed to the end of

Table 1 Double-ellipsoidal heat-source parameters

Exp. No.s	a_f	a_r	b	d
1–9	2.23	7.00	2.25	3.30
10–18	1.96	7.20	2.77	3.77
19–27	1.85	7.65	2.25	3.30

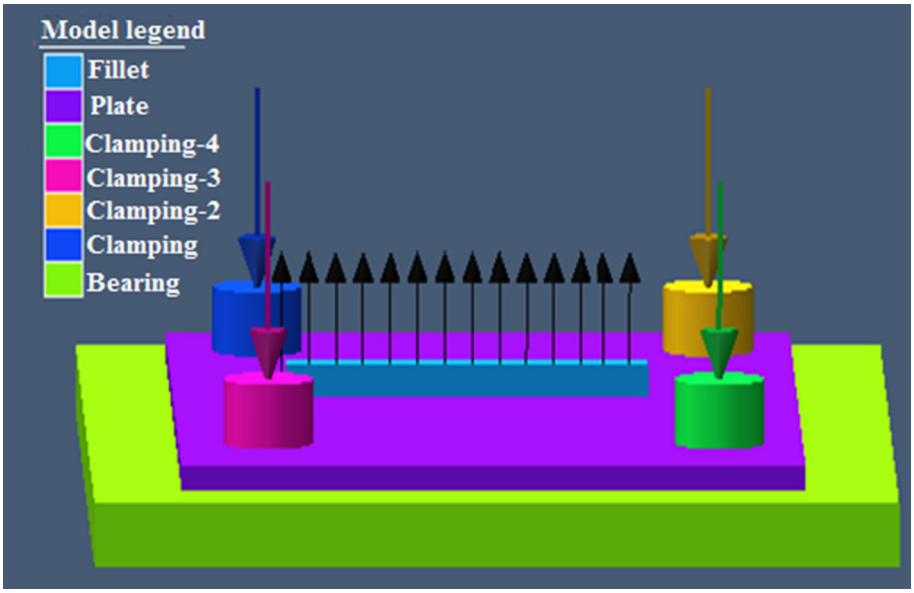

Fig. 4 Simulation of AM

the robot arm. The torch was provided with a 1.2-mm-diameter mild steel electrode and a supply of inert gas. While the electrode was deposited on the substrate, the inert gas acted as a shielding gas, protecting the metal deposition from the atmosphere.

The experiments were conducted at a current of 150 A. During the experiments, a gas mixture of 95% argon and 5% CO_2 was used as the shielding gas, with a gas flux of 25 L/min. As shown in Fig. 6, the metal was deposited on the substrate, while the torch was kept inclined at 60°, 90°, and 120°. As per design of experiments, twenty-seven experiments were conducted, with three different torch angles, wire feed speeds, and welding travel speeds, respectively, as shown in Fig. 7.

After the experiments, the substrate was removed and sectioned across the weld beads using a wire cut electric discharge machining process. As shown in Fig. 8, the size of the weld bead or the size of the metal deposition, such as the width of the weld bead (WWB), the height of the weld bead (HWB), and the penetration/depth of the weld bead (DWB), was measured using a microscope for the experiment 1. It was observed that the simulated weld geometry was found to be same as the experimental weld geometry. The measured values of the HWB, WWB and DWB for the twenty-seven experiments are presented in Table 2.

4 Results and discussion

In the present study, the effects of the welding travel speed, wire feed speed, and torch angle on the weld bead geometry (e.g. HWB, WWB and DWB) were examined. FEM-based simulations were performed for twenty-seven experiments, and the weld bead geometry was compared with experimental results. The simulated results for the widths of the weld bead and heat-affected zone (HAZ) for the first experiment, which was performed with a torch angle of 60°, a wire feed speed of 5 m/min, and a welding speed of 0.2 m/min, are shown in Figs. 9a and b, respectively. At approximately 1600 °C, heat accumulated in the weld pool, which melted the substrate, and the molten electrode metal formed the weld bead. The region around the weld pool (called the HAZ) was also affected by the heat, having a temperature as high as 1000 °C. The experimental and simulation results for the HWB, WWB and DWB were compared. The error between the experimental and simulation results was $< 5\%$.

4.1 Width of weld bead (WWB)

The WWB is one of the output characteristics that influences the dimensional accuracy of AM. The interaction effect of the process parameters on the WWB bead is shown in Fig. 10. From Fig. 10a, as the size of the weld pool was directly proportional to the size of the weld bead, the weld-bead size increased when the wire feed speed and torch angle increased from 5 to 7 m/min and from 60° to 120°, respectively. As shown in Fig. 10b, as the size of the weld pool decreased when the welding speed increased, the WWB decreased when the welding speed increased from 0.2 to 0.4 m/min. As shown in Fig. 10c, the WWB increased when the wire feed speed increased from 5 to 7 m/min and decreased, while the welding speed increased from the 0.2 to 0.4 m/min.

The effect of the torch angle on the size of the weld bead is shown in Fig. 11. Figure 11 a and b presents schematics

Table 2 Design of experiments and experimental results

Exp.No	Design of experiments			Weld bead geometry (mm)					
	TA (°)	WFS (m/min)	WS (m/min)	Exp. HWB	Sim. HWB	Exp. WWB	Sim. WWB	Exp. DWB	Sim. DWB
1	60	5	0.2	4.49	4.62	8.74	7.95	1.91	1.81
2	60	5	0.3	3.02	3.20	7.60	7.71	1.81	1.98
3	60	5	0.4	2.63	2.51	7.61	7.89	1.80	1.81
4	60	6	0.2	4.68	4.47	8.27	8.02	2.11	2.20
5	60	6	0.3	3.80	3.70	8.68	8.33	2.05	2.16
6	60	6	0.4	2.72	2.80	7.80	7.80	1.96	1.84
7	60	7	0.2	4.68	4.81	8.08	8.22	2.11	2.09
8	60	7	0.3	4.33	4.41	7.79	7.83	2.01	2.16
9	60	7	0.4	3.48	3.95	7.78	7.02	2.08	2.22
10	90	5	0.2	4.08	3.97	10.37	9.92	2.24	2.38
11	90	5	0.3	3.32	2.92	8.37	8.58	2.16	2.21
12	90	5	0.4	2.64	2.55	7.91	8.20	2.04	1.98
13	90	6	0.2	4.63	4.80	10.31	10.16	2.38	2.49
14	90	6	0.3	4.13	4.00	8.45	8.61	2.30	2.43
15	90	6	0.4	2.89	2.97	8.05	7.93	2.24	2.27
16	90	7	0.2	4.86	4.51	9.98	10.15	2.48	2.46
17	90	7	0.3	4.66	4.67	8.15	8.24	2.35	2.31
18	90	7	0.4	4.04	3.85	7.92	7.73	2.21	2.27
19	120	5	0.2	3.94	4.02	10.44	10.04	1.13	1.20
20	120	5	0.3	2.63	2.51	9.63	10.11	1.49	1.38
21	120	5	0.4	2.62	2.58	8.10	8.46	1.83	2.02
22	120	6	0.2	4.40	4.41	10.45	9.88	1.12	1.42
23	120	6	0.3	3.02	3.25	9.89	9.92	1.58	1.50
24	120	6	0.4	2.88	8.17	8.36	1.90	2.00	2.05
25	120	7	0.2	4.67	4.51	10.43	10.67	1.98	1.84
26	120	7	0.3	3.50	3.67	9.70	9.04	1.65	1.59
27	120	7	0.4	3.49	3.48	8.25	8.58	1.22	1.38

of metal deposition with torch angles of 60° and 90°, respectively. When the torch angle is 60°, the arc force is applied to the weld pool in the welding direction. As shown in Fig. 11a, the electrode molten metal was forced into the weld pool in the direction of welding, which results in reduced WWB. In addition, when the wire feed speed increased at low values of welding speed, excess electrode molten metal causes increased WWB. When the torch angle was kept at 120°, the arc force was applied to the weld pool in the direction opposite to the welding direction. As shown in Fig. 11b, the electrode molten metal was pushed over the weld bead, which results in increased WWB (Hu et al. 2018). Nitish et al. (Gokhale et al. 2019) also found increased thickness and reduced height of weld bead as the angle of torch was increased.

4.2 Height of weld bead (HWB)

The HWB determines the number of welding passes needed to build an object in AM. The interaction effect of the process parameters on HWB is presented in Fig. 12. As shown in Fig. 12a, the HWB increased as the wire feed speed increased from 5 to 7 m/min, but the HWB decreased as the torch angle increased from 60° to 120°. As shown in Fig. 12a, as the WWB increased as the torch angle increased, which reduced the HWB. As shown in Fig. 12 a and b, the HWB decreased when the welding speed increased from 0.2 to 0.4 m/min. As shown in Fig. 12c, the HWB decreased when the welding speed increased from 0.2 to 0.4 m/min at low wire feed speed (5 m/min), but the HWB increased when the wire feed speed increased from 5 to 7 m/min. At high welding speeds, the low consumption rate of the electrode metal

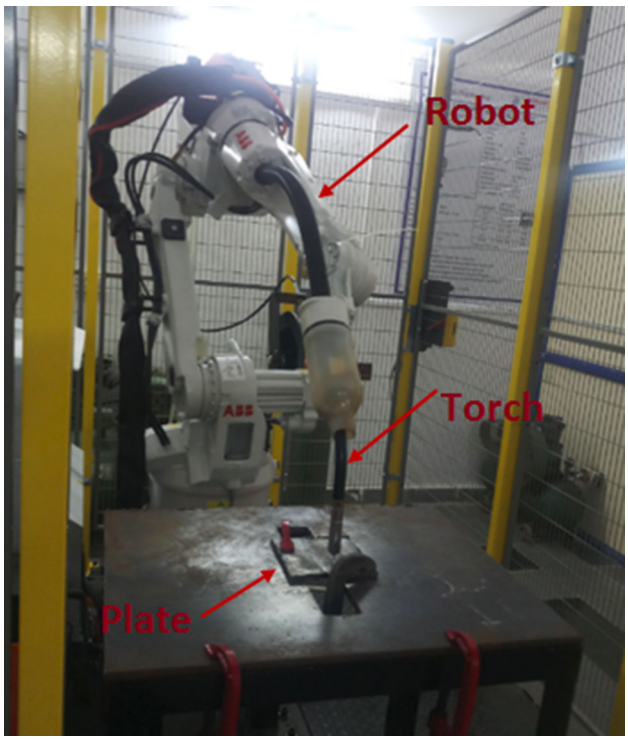

Fig. 5 Experimental setup for AM

reduced the HWB. But, excess molten metal of wire increased the HWB when the wire feed speed increased.

4.3 Depth of weld bead (DWB)

The DWB is an important output characteristic that indirectly affects the width and height of the weld bead. Higher values of the weld depth result in lower values of the HWB. As shown in Fig. 13, the torch angle and welding speed had mixed effects on the depth of the weld pool. As shown in Fig. 13a, the DWB increased as the torch angle increased from 60° to 90°and then decreased as the torch angle increased from 90° to 120°. As shown in Fig. 11, at torch angles of 60° and 120°, the arc forces were applied in the inclined direction at the weld pool, which resulted in an overflow of molten metal and a reduced DWB. Additionally, the DWB increased as the wire feed speed increased from 5 to 7 m/min at the three torch angles. As shown in Fig. 13 b and c, the DWB increased as the welding speed increased from 0.2 to 0.3 m/min and then decreased as the welding speed increased from 0.3 to 0.4 m/min. At low welding speeds, the consumption of the electrode metal was low, reducing the depth. At high welding speeds, insufficient wire was fed, reducing the DWB.

5 ANN algorithm

ANN is one of the ML techniques working with supervised learning. In supervised learning ANNs, a multi-layer perceptron (MLP) model is trained with feed-forward back-propagation algorithms. The MLP networks are the data-driven techniques capable of modelling complex tasks, where as the physics-driven modelling and mathematical modelling are difficult (Kucukoglu et al. 2018). As the ANN has strong modelling and prediction skills, they are suitable to evaluate accuracy of wall geometry in AM (Qi et al. 2019). During the supervised learning, the network was given a set of data which includes inputs and their corresponding output targets. The neurons in each layer propagate the given information until the given information

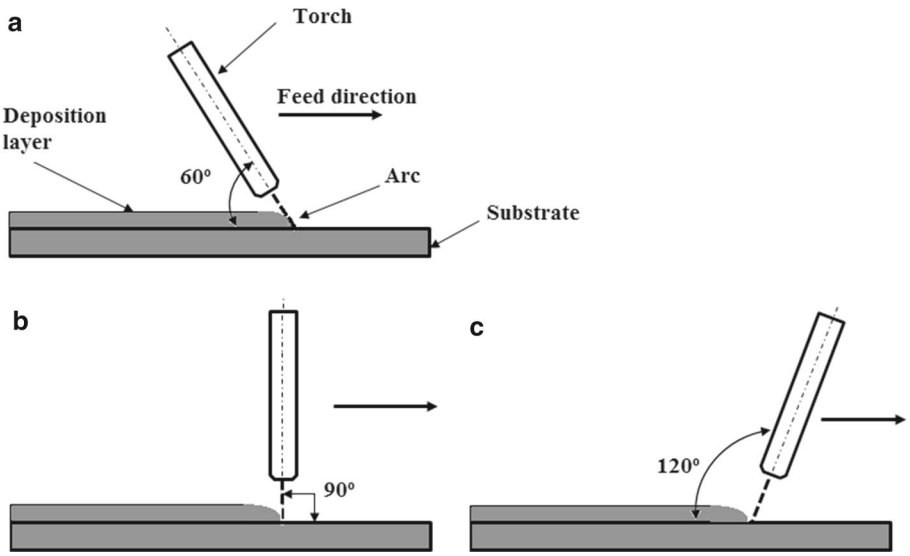

Fig. 6 Torch angles of 60°, 90°, and 120°during the metal deposition

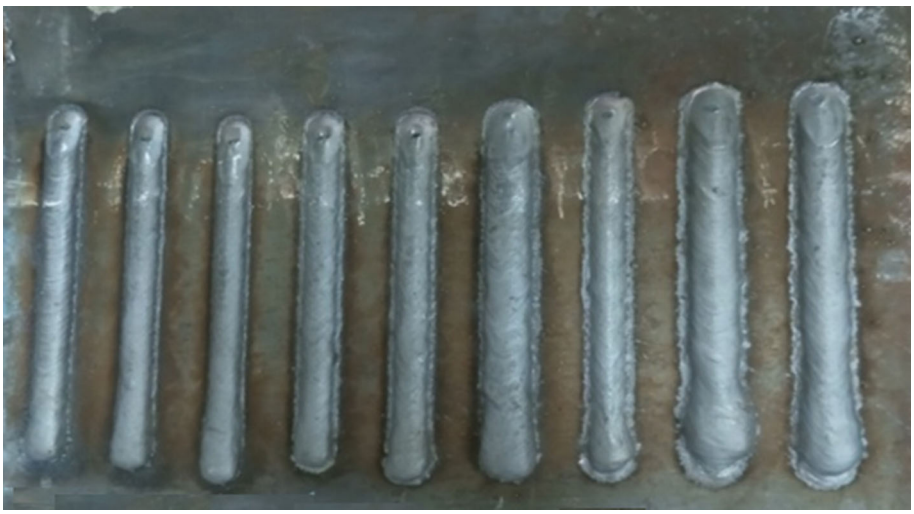

Fig. 7 Metal deposition under different working conditions

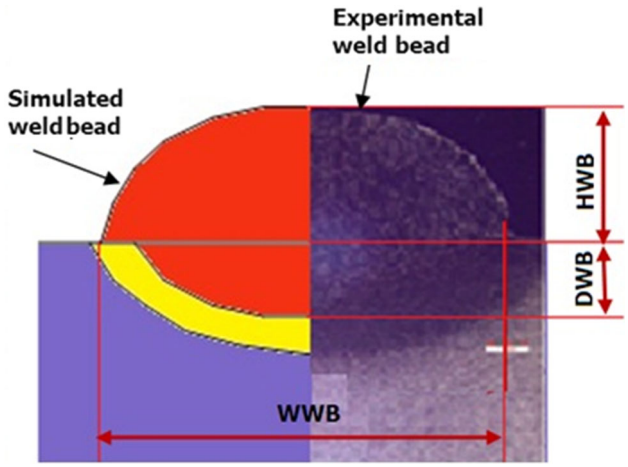

Fig. 8 Geometry of the weld bead for experiment 1

reached the neurons in the output layer. Magnitude of each neuron in the output layer was estimated using Eq. (4) (Venkata Rao and Murthy 2018; Mehrotra et al. 1997).

$$y = f\left(\sum_i w_i x_i\right) = f(w.x) = f\left(w^T x\right) \tag{4}$$

where the x represents input, and the w represents weight or efficiency of the connection. The network also calculated error between the estimated output value and the output targets. If the error was found beyond the target error, the backpropagation algorithm changed weights of the connections between the layers until the error was found less than the target error (Almeida et al. 2020).

In the present study, a feed-forward MLP network was used to model the weld/wall geometry. As shown in Fig. 14, the 3-9-3 MLP consists of three layers such as input layer, hidden layer and output layer. There are connections between the layers to transform the information between the layers. The input layer consists of three neurons or nodes such as torch angle, wire feed speed and welding speed, and the output layer consists of three neurons such as HWB, WWB and DWB. The hidden layer

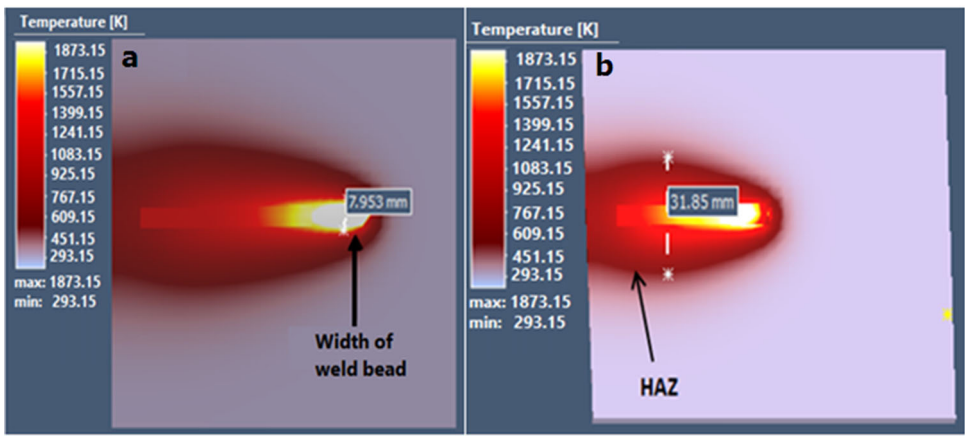

Fig. 9 Widths of weld bead, and HAZ for experiment 1

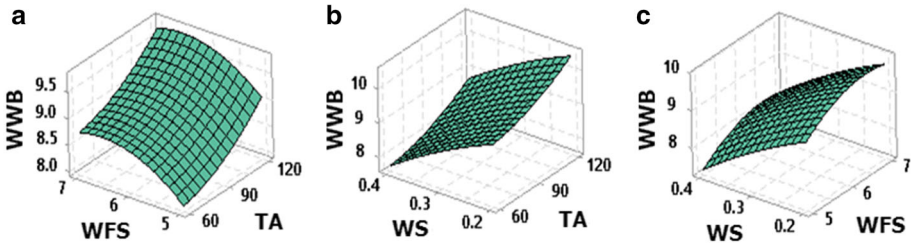

Fig. 10 Interaction effect of the process parameters on the width of the weld bead

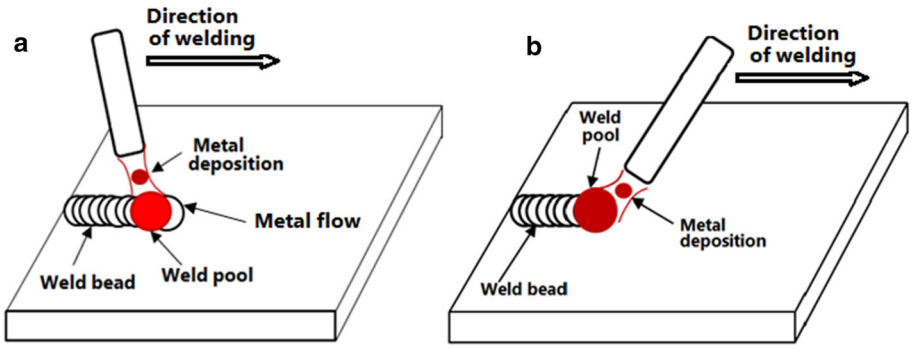

Fig. 11 Metal deposition at torch angles of 60°and 120°

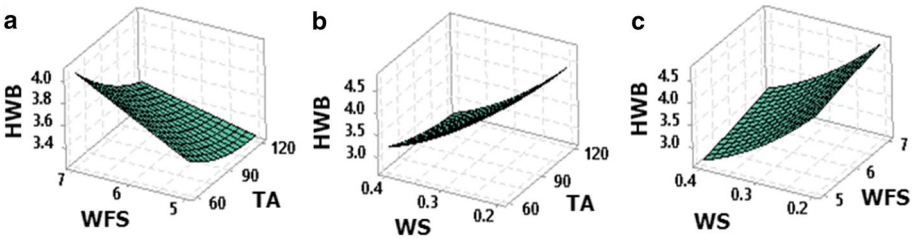

Fig. 12 Interaction effect of the process parameters on the height of the weld bead

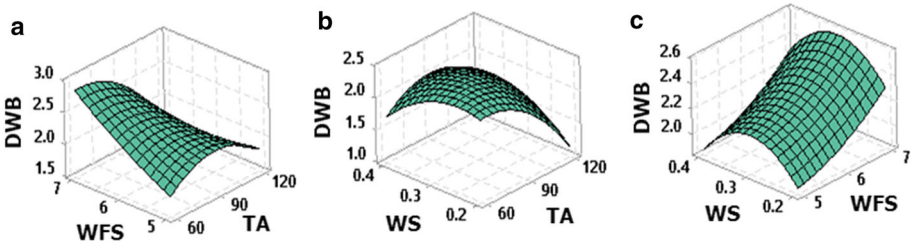

Fig. 13 Interaction effect of the process parameters on the depth of the weld bead

consists of nine neurons. Number of hidden layers and number of neurons in the hidden layer were estimated by trial and error method (Venkata Rao and Murthy 2018) based on target error. In the present study, target error was set to 0.01 during the training.

As shown in Fig. 15, the network was training with feed-forward backpropagation algorithm using EasyNN-plus software. The network was trained with the 20 samples consisting of different working conditions performed at different levels of torch angle, wire feed speed and welding speed and the corresponding height, width and depth of weld bead as presented in Table 2. During the training, the target error was set to 0.01, and the learning rate and momentum were set to 0.6 and 0.8, respectively. The network was stopped when the average training error reached to a value which is less than the target error. Since the sample size is less for training of the network, number of hidden layers and number of nodes in hidden layers were estimated by trial and error method based on the testing error. The number of hidden layers and neurons in the hidden layer were changed until the average training was found less than 0.01. In the present study, average training error (0.00002) of the 3-9-3 network was found less the target error (0.01). That is why, this network was used in the present study for modelling of the weld bead geometry. Weight of the connections between the input layer and hidden layer was selected as 21, and the weight of the connections between the hidden layer and output layer was

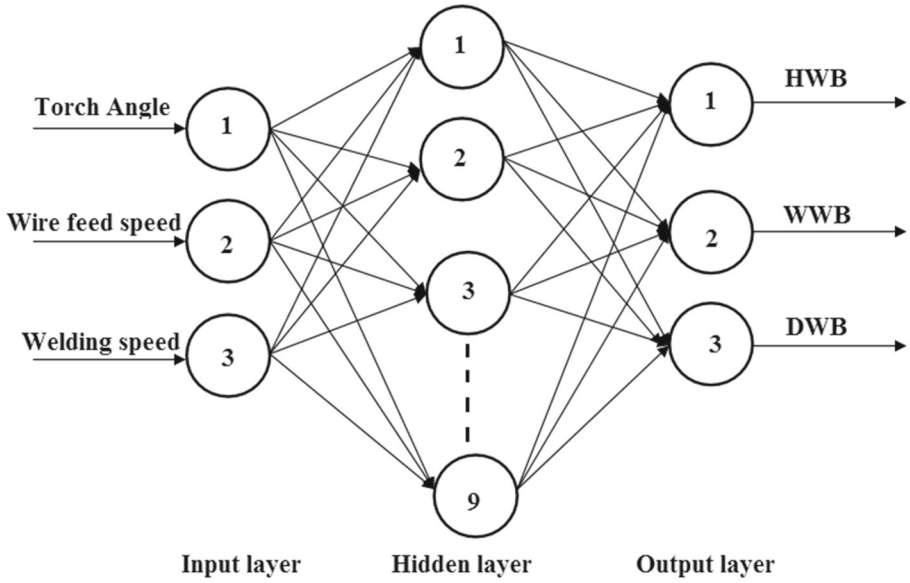

Fig. 14 A multi-layered 3-9-3 perceptron

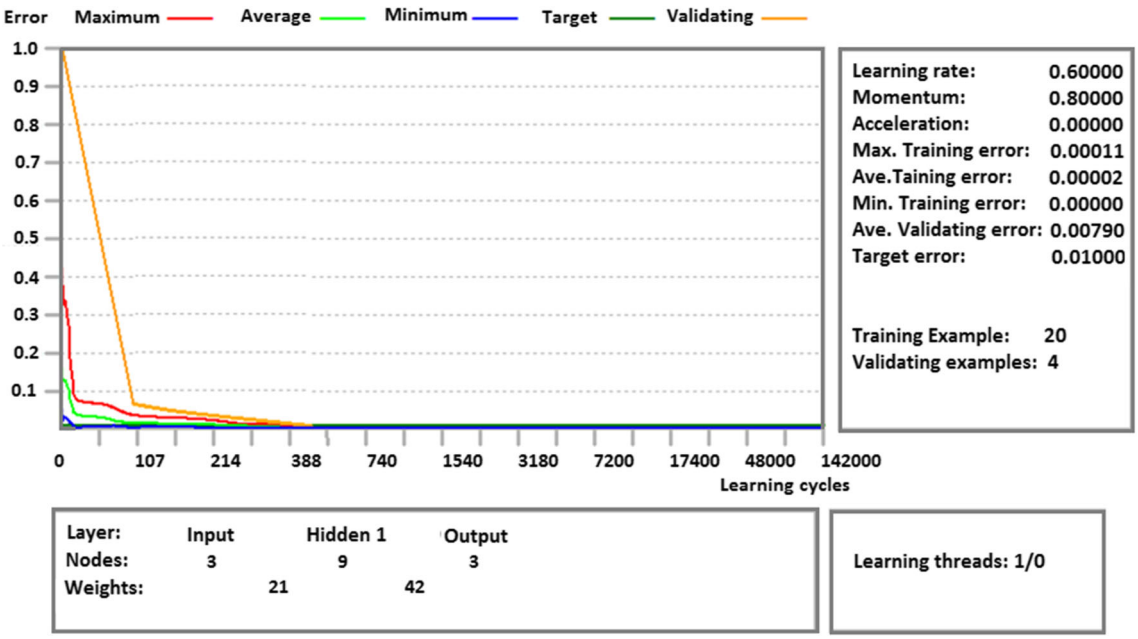

Fig. 15 Learning graph with training and validation error

Table 3 Experimental, ANN and simulation results of weld bead geometry

Exp.No	HWB (mm)			WWB (mm)			DWB (mm)		
	Exp	ANN	Sim	Exp	ANN	Sim	Exp	ANN	Sim
2	3.02	3.00	3.20	7.60	7.80	7.71	1.81	1.90	1.98
16	4.86	4.70	4.51	9.98	9.87	10.15	2.48	2.47	2.46
24	2.75	2.70	2.88	8.17	8.07	8.36	2.00	1.98	2.05

selected as 42 randomly by the software itself (Almeida et al. 2020). After training, the network was tested with experimental results as presented in Table 3.

Experimental values, ANN predicted values and numerical simulation results of the weld/wall geometry are presented in Table 3. The ANN predicted values and numerical simulation results were compared with the

experimental results, and average error was also computed for HWB, WWB and DWB. The ANN predicted values have average errors as 1.97%, 1.64% and 3.24% for HWB, WWB and DWB, respectively, with the experimental results. At the same time, the ANN predicted values have average errors as 5.96%, 1.82% and 6.93% for HWB, WWB and DWB, respectively. It was observed that the data-driven-based ML technique predicted the responses very close to the experimental results than the physics-driven modelling technique.

6 Optimisation of process parameters

The Taguchi-based GTMA and the utility concept were used to optimise the process parameters for improving the dimensional accuracy of AM. The height, width, and depth of the weld bead were taken as performance characteristics to optimise the process parameters for achieving maximum performance in AM. The GTMA was used to estimate the weights for the height, width, and depth of the weld bead, and the Taguchi method was used to obtain the preference scales for the three output characteristics. The utility concept was employed to estimate the overall utility of the three output characteristics using their weights and preference scales, as follows:

$$U = P_{\mathrm{HWB}} W_{\mathrm{HWB}} + P_{\mathrm{WWB}} W_{\mathrm{WWB}} + P_{\mathrm{DWB}} W_{\mathrm{DWB}} \tag{5}$$

where U represents the overall utility value, and P_{HWB}, P_{WWB}, and P_{DWB} represent the preference scales for the height, width, and depth of the weld bead, respectively. The W_{HWB}, W_{WWB}, and W_{DWB} represent the weights of the height, width, and depth of the weld bead, respectively.

Various steps involved in estimation of weights for the height, width and depth of weld bead were described below.

6.1 Preference graphs (PG)

Figure 16 shows the preferences given to the output characteristics by different users according to their requirement. User 1 gave high priority to the height of the weld bead, followed by the width and depth. User 2 gave equally high priority to the width and height, followed by the depth. User 3 gave high priority to the height, followed by equal priority to the width and depth. User 4 gave high priority to the width, followed by the height and depth. Based on the preferences, the preference matrices were constructed as follows:

$$\mathrm{PG}_1 = \begin{bmatrix} \mathrm{HWB} & \mathrm{WWB} & \mathrm{DWB} \\ 0 & 1 & 0 \\ 0 & 0 & 1 \\ 0 & 0 & 0 \end{bmatrix} \begin{matrix} \mathrm{HWB} \\ \mathrm{WWB} \\ \mathrm{DWB} \end{matrix}$$

$$\mathrm{PG}_2 = \begin{bmatrix} 0 & 0 & 1 \\ 0 & 0 & 1 \\ 0 & 0 & 0 \end{bmatrix} \quad \mathrm{PG}_3 = \begin{bmatrix} 0 & 1 & 1 \\ 0 & 0 & 0 \\ 0 & 0 & 0 \end{bmatrix}$$

$$\mathrm{PG}_4 = \begin{bmatrix} 0 & 0 & 1 \\ 1 & 0 & 0 \\ 0 & 0 & 0 \end{bmatrix}$$

6.2 Dominance matrix

Dominance matrices (D^{n}) for the three preference graphs were estimated as follows (K. Venkata rao 2019):

$$D^n = (PG_n)^1 + (PG_n)^2 + \ldots\ldots\ldots + (PG_n)^{m-1} \tag{6}$$

where n is the number of users, and m is the number of weld bead parameters

$$D^1 = \begin{bmatrix} 0 & 1 & 1 \\ 0 & 0 & 1 \\ 0 & 0 & 0 \end{bmatrix} \quad D^2 = \begin{bmatrix} 0 & 0 & 1 \\ 0 & 0 & 1 \\ 0 & 0 & 0 \end{bmatrix} \quad D^3 = \begin{bmatrix} 0 & 1 & 1 \\ 0 & 0 & 0 \\ 0 & 0 & 0 \end{bmatrix}$$

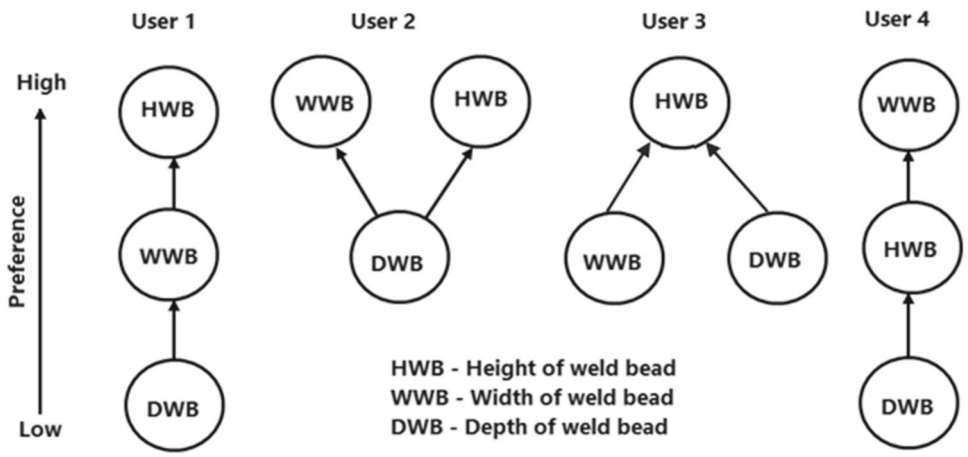

Fig. 16 Preference graph with different users' preferences of output characteristics

$$D^4 = \begin{bmatrix} 0 & 0 & 1 \\ 1 & 0 & 1 \\ 0 & 0 & 0 \end{bmatrix}.$$

6.3 Relative degree of performance

The relative degree of performance (RDP) among the three weld bead parameters was estimated using Eq. (7) (Venkata rao 2019).

$$rdp_m^n = \frac{1 + d_m^n}{\text{Max}_{m=1....M}\, 1 + d_m^n} \tag{7}$$

6.4 Relative importance rating

The relative importance rating (RIR) was estimated using Eq. (8) (Venkata rao 2019).

$$\text{RIR}_m = \frac{\sum_{n=1}^{N} rdp_m^n}{\text{Max}_{m=1....M} \sum_{n=1}^{N} rdp_m^n} \tag{8}$$

6.5 Weight

Weights (W) of the three weld bead parameters were estimated using Eq. (9) (Venkata rao 2019; Babu et al. 2017).

$$W_m = \frac{rir_m}{\sum_{m=1}^{M} rir_m} \tag{9}$$

W_m = (0.449, 0.367, 0.184)

Weights for the height, width and depth of weld bead were estimated as 0.449, 0.367 and 0.184, respectively.

In the next step, preference scales for the height, width, and depth of the weld bead were estimated. The process parameters were optimised using the Taguchi method for the three output characteristics separately. As the present study was aimed maximize HWB and minimise WWB and DWB, "larger is best" was used to estimate the signal-to-noise ratio for HWB, and "smaller is best" was used to estimate the signal-to-noise ratio for the WWB and DWB, via Eqs. (10) and (11) (Rao et al. 2016). The term signal represents desired value, and the noise represents undesired value. The optimal values of the output characteristics were predicted using the Taguchi method and are presented in Table 4. From Table 2, the maximum acceptable levels of HWB, WWB and DWB were selected, as shown in Table 4.

"Smaller is best"

$$\frac{S}{N} = -10 \log\left(\left(\frac{1}{n}\right)\left(\sum y^2\right)\right) \tag{10}$$

"Larger is best"

$$\frac{S}{N} = -10 \log\left(\left(\frac{1}{n}\right)\left(\sum \frac{1}{y^2}\right)\right) \tag{11}$$

Here, y represents the observed data, and n represents the number of samples.

6.6 Preference-scale construction

Preference scales for the three output characteristics are obtained using Eq. (12). The value of P can be selected from 0 to 9 (Kansal et al. 2006). In the present study, P was set as 9.

$$P = A \log \frac{Y'}{Y_i'} \tag{12}$$

Here, Y_i represents the predicted value of the output characteristic, Y_i' represents the maximum acceptable level of the output characteristics, and A is a constant. The value of A is estimated using optimal and acceptable levels of the output characteristics.

Preference scale for the height of the weld bead:

$$P_{\text{HWB}} = -3.35 log \frac{Y_{\text{HWB}}}{4.699} \tag{13}$$

Preference scale for the width of the weld bead:

$$P_{\text{WWB}} = -95.4 log \frac{Y_{\text{WWB}}}{7.776} \tag{14}$$

Preference scale for the depth of the weld bead:

$$P_{\text{DWB}} = 116 log \frac{Y_{\text{DWB}}}{1.121} \tag{15}$$

The weights and preference scales of the three output characteristics were substituted into Eq. (5) to calculate the combined utility value, as follows:

$$U(n, Y) = -3.35 \log \frac{Y_{HWB}}{4.699} 0.449 - 95.4 log \frac{Y_{\text{WWB}}}{7.776} 0.367 + 116 \log \frac{Y_{\text{DWB.}}}{1.121} 0.184$$

The utility values are calculated and presented in Table 5.

The process parameters were optimised to maximise the overall performance of AM using the response surface methodology. The process parameters were optimized to maximise overall quality of the weld bead, i.e. maximization of HWB and minimization of WWB and DWB. During the optimization, desirability function of the optimization was calculated using a gradient algorithm. The desirability function was estimated between 0 and 1. Desirability function with value of 1 indicates that the optimization is accepted (Venkata Rao and Murthy 2018). In the present study, the optimization was performed using MINITAB 17, and desirability function was estimated at 1

Table 4 Predicted optimal and acceptable levels of output characteristics

S. No	Output characteristics	Optimal process parameters			Predicted optimal values	Acceptable level
		Torch angle (°)	Wire feed speed (m/min)	Welding speed (m/min)		
1	HWB (mm)	60	7	0.2	4.67	4.70
2	WWB(mm)	60	5	0.4	7.08	7.78
3	DWB (mm)	120	6	0.2	1.21	1.12

Table 5 Combined utility values of three output characteristics

Exp. No	TA (°)	WFS (m/min)	WS (m/min)	Utility value
1	60	5	0.2	6.29
2	60	5	0.3	9.43
3	60	5	0.4	11.95
4	60	6	0.2	6.46
5	60	6	0.3	11.31
6	60	6	0.4	15.18
7	60	7	0.2	7.39
8	60	7	0.3	15.47
9	60	7	0.4	15.61
10	90	5	0.2	7.94
11	90	5	0.3	11.69
12	90	5	0.4	7.63
13	90	6	0.2	6.58
14	90	6	0.3	10.70
15	90	6	0.4	11.90
16	90	7	0.2	7.63
17	90	7	0.3	14.84
18	90	7	0.4	15.55
19	120	5	0.2	13.20
20	120	5	0.3	15.45
21	120	5	0.4	9.57
22	120	6	0.2	10.37
23	120	6	0.3	15.27
24	120	6	0.4	8.60
25	120	7	0.2	14.54
26	120	7	0.3	7.73
27	120	7	0.4	11.92

as shown in Fig. 17. The optimal working conditions were as follows: a torch angle of 67.4° (rounded to 68°), a wire feed speed of 6.8 m/min, and a welding speed of 0.35 m/min. Gokhale et al. (2019) also found that torch angles of $< 90°$result in better weld quality.

7 Validation of optimization

Using the optimal working conditions (torch angle of 68°, wire feed speed of 6.8 m/min, and welding speed of 0.35 m/min), the HWB, WWB and DWB were predicted using the ANN and numerical simulation methods. An experiment was also performed using the optimal working condition, where in the HWB, WWB and DWB were measured. Experimental results were compared with the ANN predicted values and numerical simulation results, and error was also estimated. The error for ANN predicted values was found to be 1.78%, 1.45% and 3.55% for HWB, WWB and DWB, respectively, and the error for the simulation results was estimated as 5.7%, 1.8% and 6.85% for HWB, WWB and DWB, respectively. The results of the three methods exhibited good agreement, as shown in Table 6. But, the ANN predicted the weld bead geometry very close to experimental values. Thus, the optimisation and the accuracy of ANN were validated experimentally.

8 Conclusions

The objective of the present study was to develop a data-driven model using machine learning technique and optimize the weld bead geometry in robotic GMAW-based AM. The torch angle was set as 60°, 90°, and 120° during experiments to examine the width, depth, and height of the weld geometry. A three-dimensional FEM was performed to examine the HWB, WWB and DWB, and width of the HAZ. In addition, ANN modelling was also performed to predict and optimize the HWB, WWB and DWB. The process parameters were optimised using the Taguchi method-based GTMA and the utility concept to improve dimensional accuracy of parts in AM. The main conclusions are drawn as follows:

- At 1600 °C, heat accumulated in the weld pool and melted the substrate, and molten electrode metal formed a weld bead. The HAZ around the weld pool was also affected by the heat up to 1000 °C.

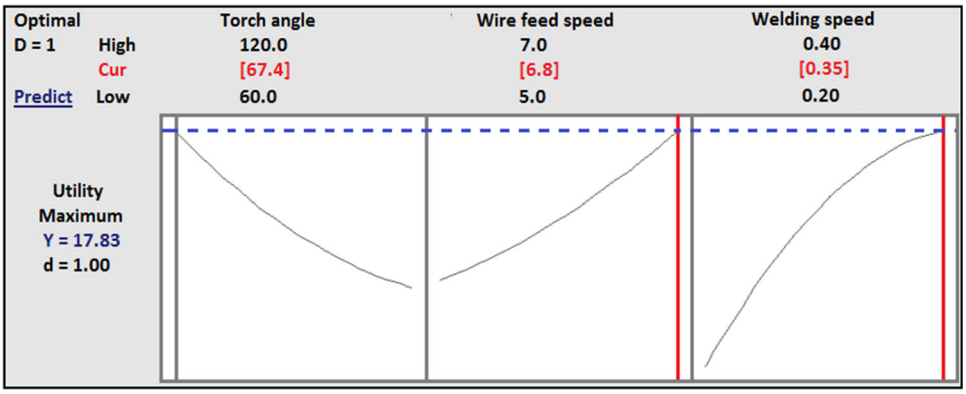

Fig. 17 Optimization of process parameters

Table 6 ANN predicted, experimental and simulated values of the weld bead geometry

HWB (mm)			WWB (mm)			DWB (mm)		
ANN	Sim	Exp	ANN	Sim	Exp	ANN	Sim	Exp
3.84	3.69	3.91	7.79	7.82	7.68	2.07	2.14	2.00

- The WWB increased as the wire feed speed and torch angle increased from 5 to 7 m/min and from 60° to 120°, respectively. As the wire feed speed increased, the consumption rate of the metal electrode increased, resulting in a larger WWB.
- When the torch angle was 60°, the arc force was applied into the weld pool in the welding direction. The electrode molten metal was pushed in to the weld pool by the arc force, which results in reduced WWB. At a torch angle of 120°, the arc force was applied to the weld pool in the direction opposite to the welding direction. The electrode molten metal was pushed over the weld bead by the arc force, which results in increased WWB.
- The HWB, WWB and DWB were predicted with ANN and numerical simulation. The ANN predicted the HWB, WWB and DWB with average errors of 1.97%, 1.64% and 3.24%, respectively. While the numerical simulation predicted the HWB, WWB and DWB with average errors of 5.96%, 1.82% and 6.93% for HWB, WWB and DWB, respectively. It was observed that the data-driven-based ML technique predicted the responses very closely with experimental results than the physics-driven modelling technique.
- The dimensional accuracy of the AM process was maximised using the proposed optimisation technique with the optimal working conditions: a torch angle of 68°, a wire feed speed of 6.8 m/min, and a welding speed of 0.3.5 m/min. Under the optimal working conditions, the height, width, and depth of the metal deposition were 3.910, 7.682, and 2.000 mm, respectively. The ANN and simulation results agreed well with the experimental results of optimum process parameters.

It was summarised that the FEM-based simulation is associated with many steps and consumes considerable amount of time in prediction of output targets. But, the ANN-based technique is able to predict the output targets in shorter time with less steps and helps to improve dimensional accuracy of parts fabricated by the AM.

Funding This work was not supported by any external funding agencies.

Declarations

Conflict of interest There are no potential conflicts of interest among the authors.

Human or animal rights As the present research was done on any human beings and animals, it does not require any informed consent/ permission from anywhere.

References

Almeida R, Goh YM, Monfared R, Steiner MTA, West A (2020) An ensemble based on neural networks with random weights for online data stream regression. Soft Comp 24:9835–9855

Azar AS (2015) A heat source model for cold metal transfer (CMT) welding. J Therm Anal Calorim 122(2):741–746

Babu GP, Murthy B, Venkatarao K, Ratnam C (2017) Multi-response optimization in orthogonal turn milling by analyzing tool vibration and surface roughness using response surface methodology. Proc Inst Mech Eng Part B J Eng Manuf 231(12):2084–2093

Cheema MS, Dvivedi A, Sharma AK (2013) A hybrid approach to multicriteria optimization based on user's preference rating. Proc Inst Mech Eng Part B J Eng Manuf 227(11):1733–1742

Chowdhury S, Mhapsekar K, Anand S (2018) Part build orientation optimization and neural network-based geometry compensation for additive manufacturing process. J Manuf Sci Eng Trans ASME 140(3):031009

Garland AP, White BC, Jared BH, Heiden M, Donahue E, Boyce BL (2020) Deep Convolutional Neural Networks as a Rapid Screening Tool for Complex Additively Manufactured Structures. Addit Manuf 35:101217

Gokhale NP, Kala P, Sharma V (2019) Thin-walled metal deposition with GTAW welding-based additive manufacturing process. J Braz Soc Mech Sci Eng 41(12):1–12

Goldak J, Chakravarti A, Bibby M (1984) A new finite element model for welding heat sources. Metall Trans B 15(2):299–305

Graf M, Hälsig A, Höfer K, Awiszus B, Mayr P (2018) Thermo-mechanical modelling of wire-arc additive manufacturing (WAAM) of semi-finished products. Metals (basel) 8(12):1009

Hu Z, Qin X, Shao T, Liu H (2018) Understanding and overcoming of abnormity at start and end of the weld bead in additive manufacturing with GMAW. Int J Adv Manuf Tech 95(5–8):2357–2368

Jin Y, Du J, He Y (2017) Optimization of process planning for reducing material consumption in additive manufacturing. J Manuf Syst 44:65–78

Kansal HK, Singh S, Kumar P (2006) Performance parameters optimization (multi-characteristics) of powder mixed electric discharge machining (PMEDM) through Taguchi's method and utility concept. Ind J Eng Mat Sci 13(3):209–216

Kim JH, Wang LS, Putta K, Haghighi P, Shah JJ, Edwards P (2019) Knowledge based design advisory system for multi-material joining. J Manuf Syst 52:253–263

Kucukoglu I, Ulusu HA, Gunduz T, Tokcalar O (2018) Application of the artificial neural network method to detect defective assembling processes by using a wearable technology. J Manuf Syst 49:163–171

Li Y, Xiong J, Yin Z (2019) Molten pool stability of thin-wall parts in robotic GMA-based additive manufacturing with various position depositions. Robot Comput Integr Manuf 56:1–11

Liu C, Law ACC, Roberson D, (James) Kong Z (2019) Image analysis-based closed loop quality control for additive manufacturing with fused filament fabrication, *J Manuf Syst,* 51: 75–86

Majeed A, Ahmed A, Lv J, Peng T, Muzamil M (2020) A state-of-the-art review on energy consumption and quality characteristics in metal additive manufacturing processes. J Braz Soc Mech Sci Eng 42(5):249

Mehrotra K, Mohan CK, Ranka S (1997) Elements of artificial neural networks. MIT Press, Cambridge

Oyama K, Diplas S, M'hamdi M, Gunnæs AE, Azar AS (2019) Heat source management in wire-arc additive manufacturing process for Al-Mg and Al-Si alloys. Addit Manuf 26:180–192

Qi X, Chen G, Li Y, Cheng X, Li C (2019) Applying neural-network-based machine learning to additive manufacturing: current applications. Chall Future Perspect Eng 5(4):721–729

Rao KV, Murthy B, Rao NM (2016) Experimental study on tool condition monitoring in boring of AISI 316 stainless steel. Proc Inst Mech Eng Part B J Eng Manuf 230(6):1144–1155

Venkata Rao K (2019) A study on performance characteristics and multi response optimization of process parameters to maximize performance of micro milling for Ti-6Al-4V. J Alloys Compd 781:773–782

Venkata Rao K, Murthy PBGSN (2018) Modeling and optimization of tool vibration and surface roughness in boring of steel using RSM, ANN and SVM. J Intell Manuf 29(7):1533–1543

VenkataRao K, Anoop Kumar T, Vidhu KP, Murthy PBGSN, NarayanaRao N, Balaji M (2016) An artificial neural network approach to investigate surface roughness and vibration of work piece in boring of AISI1040 steels. Int J Adv Manuf Tech 83(2016):919–927

Williams SW, Martina F, Addison AC, Ding J, Pardal G, Colegrove P (2016) Wire + Arc Additive Manufacturing. Mater Sci Tech 32(7):641–647

Wu D, Hua X, Ye D, Ma X, Li F (2017) Understanding of the weld pool convection in twin-wire GMAW process. Int J Adv Manuf Tech 8(1–4):219–227

Zhao H, Zhang G, Yin Z, Wu L (2011) A 3D dynamic analysis of thermal behavior during single-pass multi-layer weld-based rapid prototyping. J Mat Proc Tech 211(3):488–495

Zhao Y, Li W, Liu A (2018) Optimization of geometry quality model for wire and arc additive manufacture based on adaptive multi-objective grey wolf algorithm. Soft Comp. https://doi.org/10.1007/s00500-020-05027-y